

## Origin of the distinct site occupations of H atom in hcp Ti and Zr/Hf

Fan-Xi Yang<sup>a,b</sup>, Yi-Fei Zhu<sup>c</sup>, Shuo Cao<sup>a,\*\*</sup>, Chao-Ming Wang<sup>d</sup>, Ying-Jie Ma<sup>a</sup>, Rui Yang<sup>a</sup>, Qing-Miao Hu<sup>a,\*</sup>

<sup>a</sup> Institute of Metal Research, Chinese Academy of Sciences, Wenhua Road 72, Shenyang, 110016, China

<sup>b</sup> School of Materials Science and Engineering, University of Science and Technology of China, Jinzhai Road 96, Hefei, 230026, China

<sup>c</sup> Shenyang Dongyang Special Section Tube Co., LTD, Metallurgy 11th Road 2, Shenyang, 110000, China

<sup>d</sup> State Key Laboratory of Oil and Gas Equipment, Tubular Goods Research Institute of CNPC, Jinye 2nd Road 89, Xi'an, 710077, China



### ARTICLE INFO

**Keywords:**

hcp metals

Hydrogen embrittlement

Hydrogen storage

DFT calculations

Site occupation of H

### ABSTRACT

The location of the H atoms in Ti, Zr, and Hf is crucial to the formation of the hydrides in these metals as it influences the crystal lattice transformation and the hydrogen diffusion involved in the hydride formation process. Although Ti, Zr, and Hf are all of hexagonal close-packed structure with similar lattice parameters, the solute H atom occupies the octahedral interstice in Ti but the tetragonal interstice in Zr and Hf, of which the origin is still mysterious. In the present work, the origin of the distinct site occupation behavior of H atom in Ti and Zr/Hf is investigated through first principles calculations. The calculated solution energies confirm that H prefers the octahedral interstice in Ti but the tetrahedral interstice in Zr and Hf. We ascribe the distinct site occupations of H in Ti and Zr/Hf to the varying Coulomb repulsion between the H (as a screened proton in the metals) and the matrix atoms against the interstitial size. The competition between the H-induced electron accumulation effect and the matrix atom debonding effect might matter as well. We propose that, as a general rule, a H atom prefers the site with a trade-off between a large space and a high electron density in metals.

### 1. Introduction

Hydrogen (H) embrittles titanium (Ti) and zirconium (Zr) metals and their alloys [1–3] through the formation of brittle hydride, enhancing the atomic decohesion, accelerating the emission, multiplication, and motion of dislocations [4–7]. The behavior of hydrogen in Ti and Zr based alloys is of fundamental interest and vital importance because these alloys are the key engineering materials for aerospace, marine, and energy resource applications [8,9].

The H atoms in solid solute state reside in the interstitial sites of the crystal lattice of the metals. In Zr, the H atom was determined to occupy the tetrahedral (T) interstice at room temperature by Narang et al. [10] and Fukai [11] using the inelastic neutron scattering experiments, which was afterward confirmed by many first principles calculations based on density functional theory (DFT) [12–15]. The experimental investigation of H occupation in Hf is scarce. DFT calculations predicted that the T-site is preferable for H to occupy in Hf [16–18], similar to the case of Zr. The site occupation of H in Ti is, however, controversial. Based on their inelastic neutron scattering measurements, Khoda-Bakhsh and

Ross concluded that H locates in the T-site of Ti at temperature of 315 °C [19]. The neutron diffraction experiment by Pinto et al. [20] and the nuclear magnetic resonance measurements by Korn et al. [21] suggested that H dissolved in Ti randomly in the T-sites at room temperature as well. However, the neutron scattering experiments by Hempelmann and Stritzker [22] indicated that a large part of H atoms occupies the octahedral (O) interstices in Ti around 300 °C, in agreement with the finding of Alperin et al. [23]. Besides, advanced DFT calculations predicted consistently that H atom energetically prefers the O-site in Ti [24,25].

The possible different site occupation behavior of solute H atom in Ti and Zr/Hf as a fundamental issue is highly interesting and somehow unexpected because all three metals are of hexagonal close packed (hcp) structure and their lattice parameters  $c/a$  are very close to each other, and, therefore, their relative interstitial sizes are almost identical. More practically, the different locations of solute H are crucial to the understanding of the formation of the hydrides. Ti/Zr/Hf hydrides form through two accompanying processes, i.e., the transition of the crystal lattice from hcp to fcc (face-centered cubic) or fct (face-centered tetragonal) and the diffusion of the H atoms [26–31]. For both Ti and Zr

\* Corresponding author.

\*\* Corresponding author.

E-mail addresses: [scao14b@imr.ac.cn](mailto:scao14b@imr.ac.cn) (S. Cao), [qmhu@imr.ac.cn](mailto:qmhu@imr.ac.cn) (Q.-M. Hu).

**Table 1**

Solution energies of H in Ti, Zr, and Hf calculated with various types of exchange-correlation functionals.  $E_{\text{sol}}^{\text{T}}$  and  $E_{\text{sol}}^{\text{O}}$  are respectively the solution energies of H in tetrahedral and octahedral interstices while  $\Delta E_{\text{sol}}^{\text{O-T}}$  is the difference between them. The unit of the solution energy is eV/(H atom).

		PBE	PBESol	PW91	RPBE	Exp.
Ti	$E_{\text{sol}}^{\text{T}}$	-0.416	-0.498	-0.377	-0.175	-0.55 [11]
	$E_{\text{sol}}^{\text{O}}$	-0.515	-0.618	-0.454	-0.254	
	$\Delta E_{\text{sol}}^{\text{O-T}}$	-0.099	-0.120	-0.077	-0.078	/
Zr	$E_{\text{sol}}^{\text{T}}$	-0.427	-0.477	-0.463	-0.327	-0.42 [11,57]
	$E_{\text{sol}}^{\text{O}}$	-0.376	-0.469	-0.404	-0.193	
	$\Delta E_{\text{sol}}^{\text{O-T}}$	0.051	0.008	0.060	0.135	/
Hf	$E_{\text{sol}}^{\text{T}}$	-0.356	-0.572	-0.411	-0.250	-0.40 [11]
	$E_{\text{sol}}^{\text{O}}$	-0.255	-0.471	-0.293	-0.124	
	$\Delta E_{\text{sol}}^{\text{O-T}}$	0.101	0.101	0.118	0.126	/

**Table 2**

Lattice constants ( $a$  and  $c$ ) and sizes of the octahedral and tetrahedral interstitial site ( $d^{\text{O}}$  and  $d^{\text{T}}$ ) of Ti, Zr, and Hf calculated with GGA-PBE functional. The values listed in the parenthesis are from the experimental measurements [58].

	Ti	Zr	Hf
$a$ (Å)	2.937 (2.940)	3.231 (3.229)	3.202 (3.190)
$c$ (Å)	4.655 (4.680)	5.192 (5.141)	5.062 (5.043)
$d^{\text{O}}$ (Å)	2.074	2.272	2.240
$d^{\text{T}}$ (Å)	1.797	1.968	1.941

**Table 3**

Volume expansion induced by H in the octahedral and tetrahedral sites of Ti, Zr, and Hf calculated with GGA-PBE and supercell size of  $4 \times 4 \times 2$ .

	Ti-H	Zr-H	Hf-H
$\Delta V^{\text{O}}$	0.19	0.12	0.09
$\Delta V^{\text{T}}$	0.28	0.27	0.16

**Table 4**

Distortion energies of the Ti-H, Zr-H, and Hf-H systems (eV/s.c.) induced by a H atom in the O- ( $\Delta E_{\text{dis}}^{\text{O}}$ ) or T-site ( $\Delta E_{\text{dis}}^{\text{T}}$ ) calculated with GGA-PBE and supercell size of  $4 \times 4 \times 2$  supercell.

	Ti-H	Zr-H	Hf-H
$\Delta E_{\text{dis}}^{\text{O}}$	0.072	0.038	0.049
$\Delta E_{\text{dis}}^{\text{T}}$	0.112	0.071	0.076

hydrides, the H atoms were detected to locate in the T-sites of the fcc or fct lattice [29,32–34], regardless of the chemical stoichiometry of the hydrides. The site-occupation of H influences the hydride formation process by affecting the hcp-fcc/fct lattice transition and the diffusion of the H atom. Therefore, it is important to reveal the origin of the distinct site occupations of H in Ti and Zr/Hf.

In this paper, first-principles calculations are performed to explore the physics underlying the distinct site-occupations of H in Ti and Zr/Hf. The solution energies of H in the T and O interstices of Ti, Zr, and Hf are calculated and compared to determine the stable occupation site of H. The lattice structures and electronic structures of the systems are analyzed, with which the distinct site occupations are discussed. The paper is arranged as follows. In Section 2, we describe the method and computational details. In Section 3, we present the solution energy, crystal structure, and electronic structure from the calculations. In Section 4, we discuss the physical origin of the distinct site occupations of H in Ti and Zr/Hf. Finally, we conclude our work in Section 5.

As strongly requested by the reviewers, here we cite some references [35–47] although they are completely irrelevant to the present work.

## 2. Method and computational details

The stable occupation site of solute H in the Ti, Zr, and Hf is determined by comparing the solution energies of H in the O- and T-sites. The solution energy of a H atom is defined as

$$E_{\text{sol}} = E_{\text{M-H}} - E_{\text{M}} - \frac{1}{2}E_{\text{H}_2} \quad (1)$$

where  $E_{\text{M-H}}$ ,  $E_{\text{M}}$  and  $E_{\text{H}_2}$  are respectively the total energies of the supercell of M (M = Ti, Zr, Hf) containing one H atom, H-free M supercell, and the  $\text{H}_2$  molecule. A lower solution energy corresponds to a more stable occupation state. We adopt  $4 \times 4 \times 2$  times of the hcp unit cell to calculate the solution energy.  $E_{\text{H}_2}$  is calculated with a  $\text{H}_2$  molecule in a vacuum box with size of  $15 \text{ \AA} \times 15 \text{ \AA} \times 15 \text{ \AA}$ , which is  $-6.76 \text{ eV}$  from our calculation. The geometries, including the lattice parameter and atomic positions, of the supercells are fully optimized. In principle, the lattice vibration influences the solution energy and the site occupancy of H as well. However, we focus ourselves on the electronic structure mechanisms for the various site occupation states of H in Ti, Zr, and Hf where the lattice vibration is not involved. Therefore, we do not consider the lattice vibration energy in the present work.

Because H atom occupies the interstitial sites, relatively large local lattice distortion occurs. The sizes of the O and T interstices are different. Thus, the insertion of H results in different local lattice distortion. To measure the contribution of the local lattice distortion to the solution energy, we define the lattice distortion energy (or strain energy)  $\Delta E_{\text{dis}}$  as

$$\Delta E_{\text{dis}} = E_{\text{M-H-free}}^{\text{H-free}} - E_{\text{M}} \quad (2)$$

Here,  $E_{\text{M-H-free}}^{\text{H-free}}$  is the single point total energy of the relaxed H-containing supercell with the H atom removed.

The first-principles total energies are calculated with the first principles plane wave method based on the density functional theory (DFT) implemented in the Vienna ab initio simulation package (VASP) [48]. The projector augmented wave (PAW) pseudopotentials [49] is employed for the electron-ion interaction. The calculations are performed with various types of exchange-correlation (XC) functionals, including Perdew-Burke-Ernzerhof (PBE) [50], revised PBE for solids (PBESol) [51], Perdew-Wang (PW91) [52], and revised PBE from Hammer et al. (RPBE) [53]. The cutoff energy is set as  $500 \text{ eV}$ ,  $450 \text{ eV}$ , and  $500 \text{ eV}$  for Ti, Zr and Hf, respectively. The Monkhorst-Pack  $k$ -point grid is used to sample the reduced Brillouin zone. The density of the  $k$  points is set as about  $\sim 0.030 \text{ \AA}^{-1}$ , which is changed to about  $0.011 \text{ \AA}^{-1}$  for the calculation of density of states (DOS) calculation to obtain higher resolution of DOS. The tolerance for the electronic and ionic minimization are respectively set as  $1 \times 10^{-6} \text{ eV}$  and  $0.01 \text{ eV}/\text{\AA}$ .

The DOS and bonding charge density are calculated to analysis the electronic structures of the M – H systems. Besides, the crystal orbital Hamilton population (COHP) LOBSTER package [54,55], a tool to reconstruct electronic structures through projection of PAW-based wave functions onto atomic-like basis sets. The basis set for each calculation used recommended basis functions, which include Ti (3d, 3p, 3s, 4s), Zr (4d, 5s), Hf (6s, 5d) and H (1s).

## 3. Results

### 3.1. Solution energy of H

The solution energies of H in Ti, Zr, and Hf, calculated with various types of exchange-correlation functionals, are listed in Table 1. As seen in Table 1, all the XC functionals generate consistently lower solution energies of H in O-site ( $E_{\text{sol}}^{\text{O}}$ ) than those in T-site ( $E_{\text{sol}}^{\text{T}}$ ) for Ti, suggesting that H prefers the O-site. This prediction supports the experiments by Hempelmann and Stritzker [22] and Alperin et al. [23] but in contrast to those by Khoda-Bakhsh and Ross [19], Pinto et al. [20], and Korn et al. [21]. The solution energy difference between the O- and T-site H atoms,

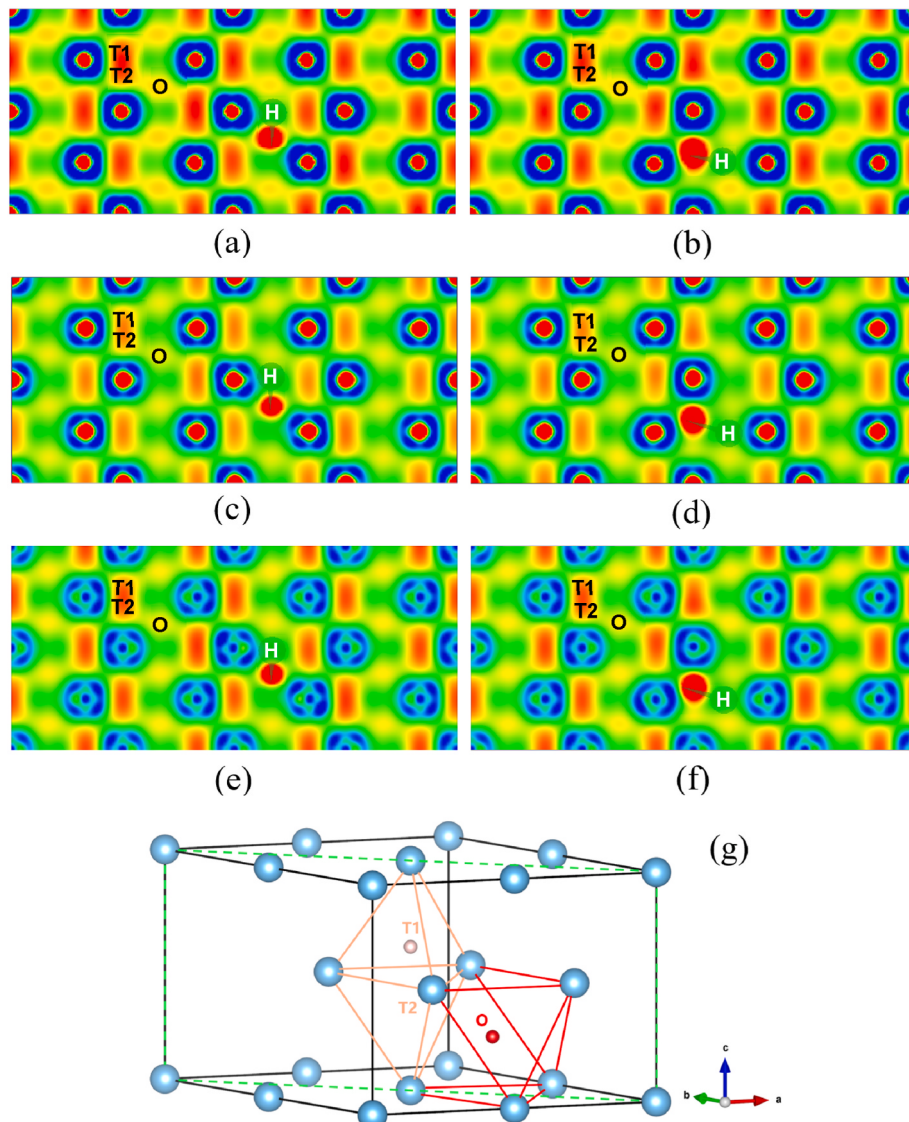


**Fig. 1.** Bonding electron density of Ti-H (a and b), Zr-H (c and d), and Hf-H (e and f) on the  $(11\bar{2}0)$  plane with H in octahedral (a, c, and e) and tetrahedral (b, d, and f) interstices, scaled from  $-0.015$  to  $0.015 \text{ e}/\text{\AA}^3$  with color from blue to red. Subfigure (g) shows the  $(11\bar{2}0)$  plane (denoted with the green dashed lines) and the H atoms in the tetrahedral and octahedral interstices (denoted respectively with the pink and red lines) in the hcp cell ( $2 \times 2 \times 1$ ). (For interpretation of the references to color in this figure legend, the reader is referred to the Web version of this article.)

$\Delta E_{\text{sol}}^{\text{O-T}}$ , is about  $-0.10 \pm 0.02 \text{ eV}/(\text{H atom})$ . It is noted that  $\Delta E_{\text{sol}}^{\text{O-T}}$  calculated by Liang and Gong [56] is only about  $0.03 \text{ eV}/(\text{H atom})$ , with which they proposed that H atoms may occupy both the O- and T-sites in  $\alpha\text{-Ti}$ .

For Zr and Hf, all the XC functionals predict lower  $E_{\text{sol}}^{\text{T}}$  than  $E_{\text{sol}}^{\text{O}}$  with  $\Delta E_{\text{sol}}^{\text{O-T}}$  about  $0.07 \pm 0.06 \text{ eV}/(\text{H atom})$  for Zr and  $0.11 \pm 0.01 \text{ eV}/(\text{H atom})$  for Hf, indicating that H prefers the T-site. The determined site preference of H in Zr and Hf is in agreement with the experimental findings [11,57] and other theoretical predictions [12–18].

As seen in Tables 1 and in general, the PBE solution energies (in eV/(H atom) for H in its stable interstitial sites ( $-0.515$  for Ti,  $-0.427$  for Zr, and  $-0.356$  for Hf) are in better agreement with the experimental values ( $-0.55$  for Ti,  $-0.42$  for Zr, and  $-0.40$  for Hf [11,57]) than those calculated with other XC functionals. Therefore, in the following subsections, we report only the GGA-PBE results.

### 3.2. Sizes of the tetrahedral and octahedral interstices

The site preference of the light atoms such as C, N, O in the inter-

stitial sites of a metal were generally ascribed to the relative size of the interstitial sites. In general, the light atoms prefer to occupy the interstitial site with larger size. Here, we measure the size of the interstice in the hcp structure with the distance between the center of the interstitial polyhedron and its vertices, which is

$$d^{\text{T}} = \sqrt{\frac{a^2}{3} + \left(\frac{c}{4} - \frac{a^2}{3c}\right)^2} \quad (3)$$

for the T-site and

$$d^{\text{O}} = \sqrt{\frac{a^2}{3} + \frac{c^2}{16}} \quad (4)$$

for the O-site. The center of the interstitial polyhedron is defined as the position with equidistance to the vertices.

In Table 2, we list the lattice constants and sizes of the O- and T-sites of Ti, Zr, and H calculated with GGA-PBE functional. The calculated lattice constants  $a$  and  $c$  of Ti are respectively  $2.937 \text{ \AA}$  and  $4.655 \text{ \AA}$ , apparently smaller than those of Zr ( $3.231 \text{ \AA}$  and  $5.192 \text{ \AA}$ ) and Hf ( $3.195 \text{ \AA}$  and  $5.051 \text{ \AA}$ ). The calculated lattice constants of Ti, Zr, and Hf are in

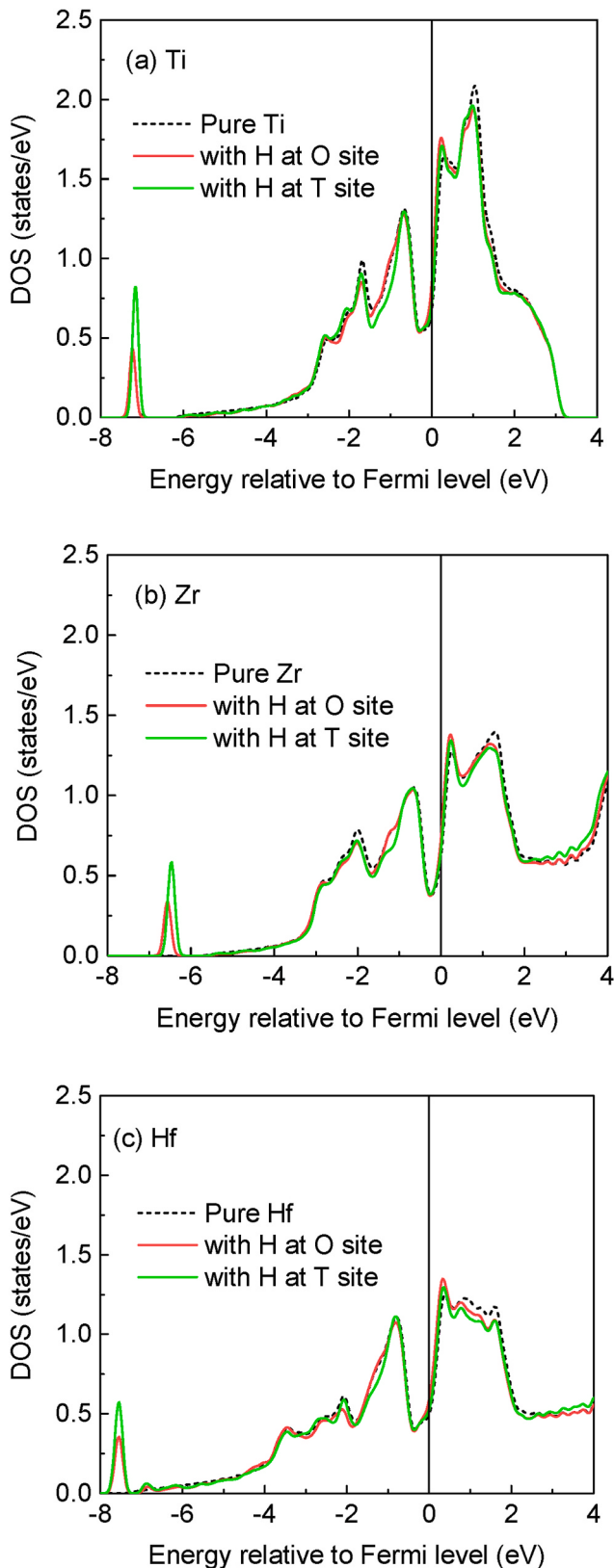


**Fig. 2.** Electronic density of states of the metal atom nearest neighboring to the H atom in octahedral (red solid line) or tetrahedral interstice (green solid lines), in comparison to that of the atom in pure metal (black dash line), (a) for Ti, (b) for Zr, and (c) for Hf. (For interpretation of the references to color in this figure legend, the reader is referred to the Web version of this article.)

good agreement with the values from experimental measurements [58]. The sizes of the O- and T-sites of Ti (2.074 Å and 1.797 Å) are smaller than those of Zr (2.273 Å and 1.968 Å) and Hf (2.235 Å and 1.936 Å).

### 3.3. H-induced volume expansion and lattice distortion energy

To further evaluate the interstitial size effect on the site occupation of H, the volume expansion and lattice distortion energy induced by the insertion of H are calculated and presented in Table 3. The volume expansion is expressed as

$$\Delta V^{O/T} = \frac{V^{O/T} - V_0}{V_0} \quad (5)$$

with  $V^{O/T}$  being the equilibrium volume of the  $4 \times 4 \times 2$  supercell containing a H atom in the O- or T-site and  $V_0$  being the volume of the supercell without H atom. As seen in Table 3, the T-site H induces larger volume expansion than the O-site one for all three metals because the T-site is smaller than the O-site one (Table 2).

In Table 4, we list the H-induced distortion energy of the Ti-H, Zr-H, and Hf-H systems. For all three systems, the distortion energy induced by T-site H,  $\Delta E_{\text{dis}}^T$ , is higher than that by O-site H,  $\Delta E_{\text{dis}}^O$ , in agreement with the larger volume change by the T-site H than that by the O-site H (Table 3). This is reasonable because the T-site is smaller than the O-site (Table 2) such that the distortion of the lattice is heavier for the T-site H than that for the O-site H. Both the distortion energies  $\Delta E_{\text{dis}}^T$  and  $\Delta E_{\text{dis}}^O$  for Ti-H are larger than the corresponding distortion energies of Zr-H and Hf-H, which may be ascribed to the more compact structure of Ti as shown by its smaller lattice constants.

### 3.4. Electronic structures

In general, the solution of H in a metal incorporates the energy loss due to the lattice distortion (lattice distortion energy or strain energy) and the energy gain due to the formation of the M – H bonds (the chemical energy) [59,60]. The strain/distortion energy have already been presented in subsection 3.3. In this subsection, we focus ourselves on the chemical aspect by analyzing the bonding electron density, electronic density of states, and the COHP.

#### 3.4.1. Bonding electron density

The bonding electron density is evaluated as the difference between the self-consistent electron density and the superposition of the atomic electron density, which describes the redistribution of the electrons due to the formation of a crystal from free atoms. Fig. 1 displays the bonding electron densities on the  $(11\bar{2}0)$  planes of Ti, Zr, and Hf with H in O and T interstices. For the pure metals, the bonding electrons mainly distribute in the interstitial sites (labeled as T1, T2, and O in Fig. 1) of the crystal. The bonding electron density in the T interstice (e.g., T1 and T2) is much higher than that in the O interstice (e.g., labeled as O in Fig. 1). This is reasonable because the T interstice is surrounded by the nearest neighboring metal atoms whereas the O interstice is more open (see Fig. 1g). The bonding electron density of Ti (Fig. 1a and b) is discernibly higher than those of Zr and Hf (Fig. 1c–f).

When a H atom is inserted into the interstice, the electrons in the interstice accumulate around the H atom. Especially for H at the T-site, the electrons in the H-locating T interstice and the one next to it are attracted to the H atom, making the latter T interstice depletion of electrons (see Fig. 1b, d and 1f). There are more electrons around the T-site H than the O-site H because, on the one hand, the electron density in the T interstice is higher than that in the O interstice, on the other hand, the electrons in two neighboring T interstices are attracted to the H in one of them as depicted above. For both the O and T interstices, the electron accumulation around H in Ti is more significant than that in Zr and Hf.

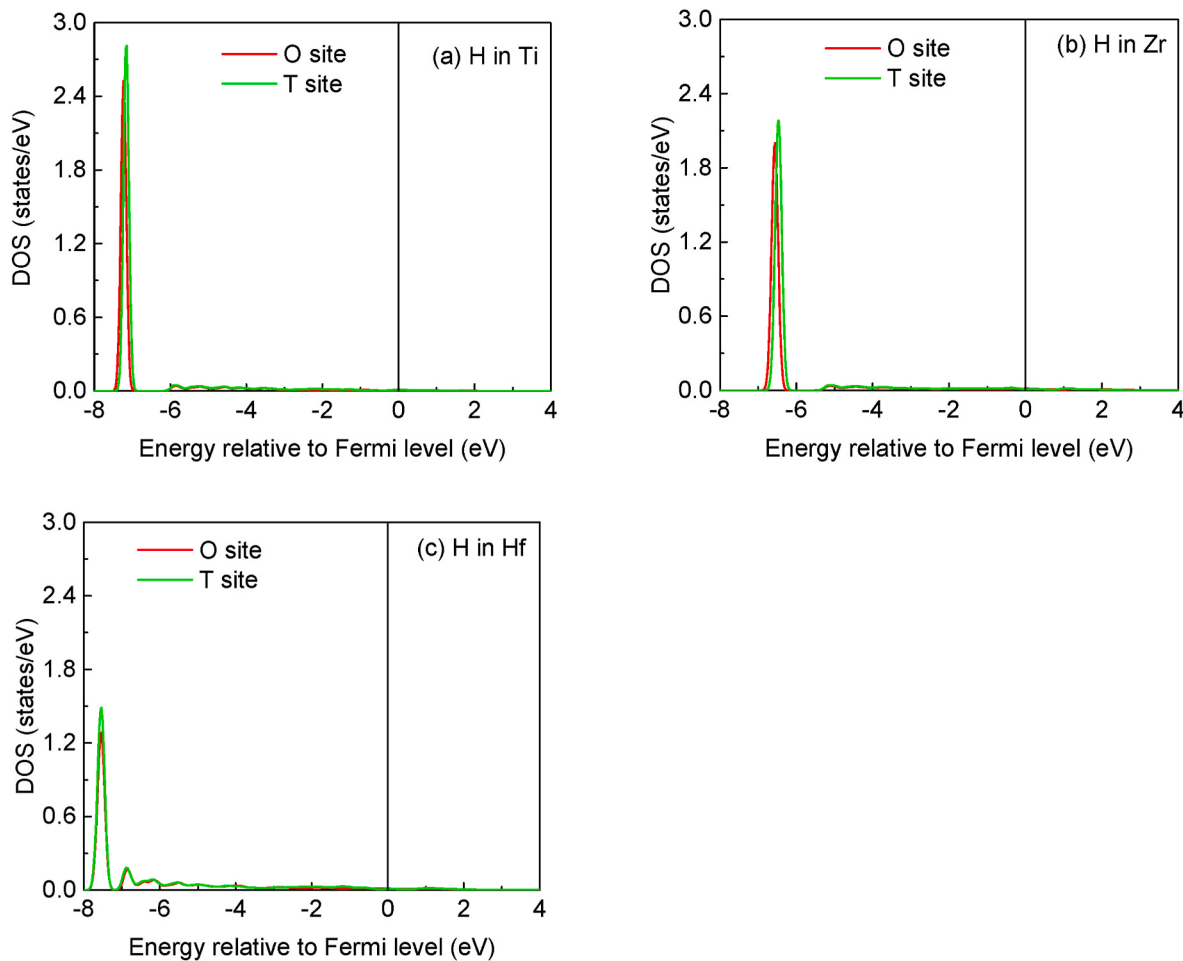


**Fig. 3.** Electronic density of states of H atoms in the tetragonal and octahedral interstices of Ti (a), Zr (b), and Hf (c).

#### 3.4.2. Electronic density of states

Fig. 2 compares the local electronic density of states (DOS) of the metal atom in pure crystal and the one nearest neighboring to the H atom in Ti-H, Zr-H, and Hf-H solutions. It is seen that the insertion of the H atoms into the crystal induces a low-lying state in the DOS of the metal atom, located respectively at about -7.2 eV, -6.6 eV, -7.5 eV for Ti, Zr, and Hf. The low-lying state of the metal atom with nearest neighboring T-site H is higher than that for the metal atom with nearest neighboring O-site H for all three systems. Except for the low-lying state, the major parts of the DOSs of the metal atom with nearest neighboring O- and T-site H as well as the one without neighboring H are hardly discernible.

Fig. 3 displays the DOS of H in O- and T-sites of Ti, Zr, and Hf. It is seen that a sharp low-lying peak appears at about -7.2 eV, -6.6 eV, -7.5 eV for Ti, Zr, and Hf for both the O- and T-site H. The positions of the low-lying states of H in Ti, Zr, and Hf are in consistent with those of the low-lying states of its nearest neighboring host metal atoms. The peak for the T-site H is higher than that for the O-site H. The coincidence between the low-lying state of the metal and that of the H atom indicates that there exists covalent interaction between the metal and H atoms.

#### 3.4.3. Crystal orbital Hamilton population

As compared to the bonding electron density and DOS, the crystal orbital Hamilton population provides some additional information about the atomic bonding characters. Fig. 4 displays the -COHPs of the shortest M-H bonds with the H atom occupying O- or T-sites in Ti, Zr, and Hf. For all three systems, -COHP is negative above energy level of about -3 eV, indicating that the corresponding electronic states are

antibonding characterized. -COHP below about -3 eV is positive such that the corresponding electronic states are bonding characterized. The antibonding character for the T-site H is slightly stronger than that for the O-site as the -COHP for the O-site H is a little bit more negative than that for the T-site H.

## 4. Discussion

Our first principles calculations of the solution energies demonstrate that the H atom prefers the O-site in Ti but the T-site in Zr and Hf (see Table 1). However, the three systems share the same geometric and electronic structure characteristics: (1) smaller size of the T interstice than that of the O interstice (Table 2); (2) larger distortion energy induced by the T-site H than that by the O-site H (Table 4); (3) higher electron density around the T-site H than that around the O-site H (Fig. 1); (4) higher low-lying DOS for the T-site H than that for the O-site H (Figs. 2 and 3); (5) slightly stronger antibonding character of the M – H bond for the O-site H than that for the T-site H (Fig. 4). Such similarities among the three systems make it hard to tell why the H atom prefers the O-site in Ti but the T-site in Zr and Hf. Nevertheless, we notice that the size of the interstice in Ti is significantly smaller than that in Zr and Hf because the Ti is more compact (i.e., smaller lattice constants) than Zr and Hf (see Table 2). With this observation, we present an explanation on the distinct site occupations of H in Ti and Zr/Hf considering the nature of H in transition metals.

The nuclear-magnetic-resonance study of H atom in early transition metals suggested convincingly that the H atom exists as a proton in metals [61]. The electrons tend to cluster around the proton such that

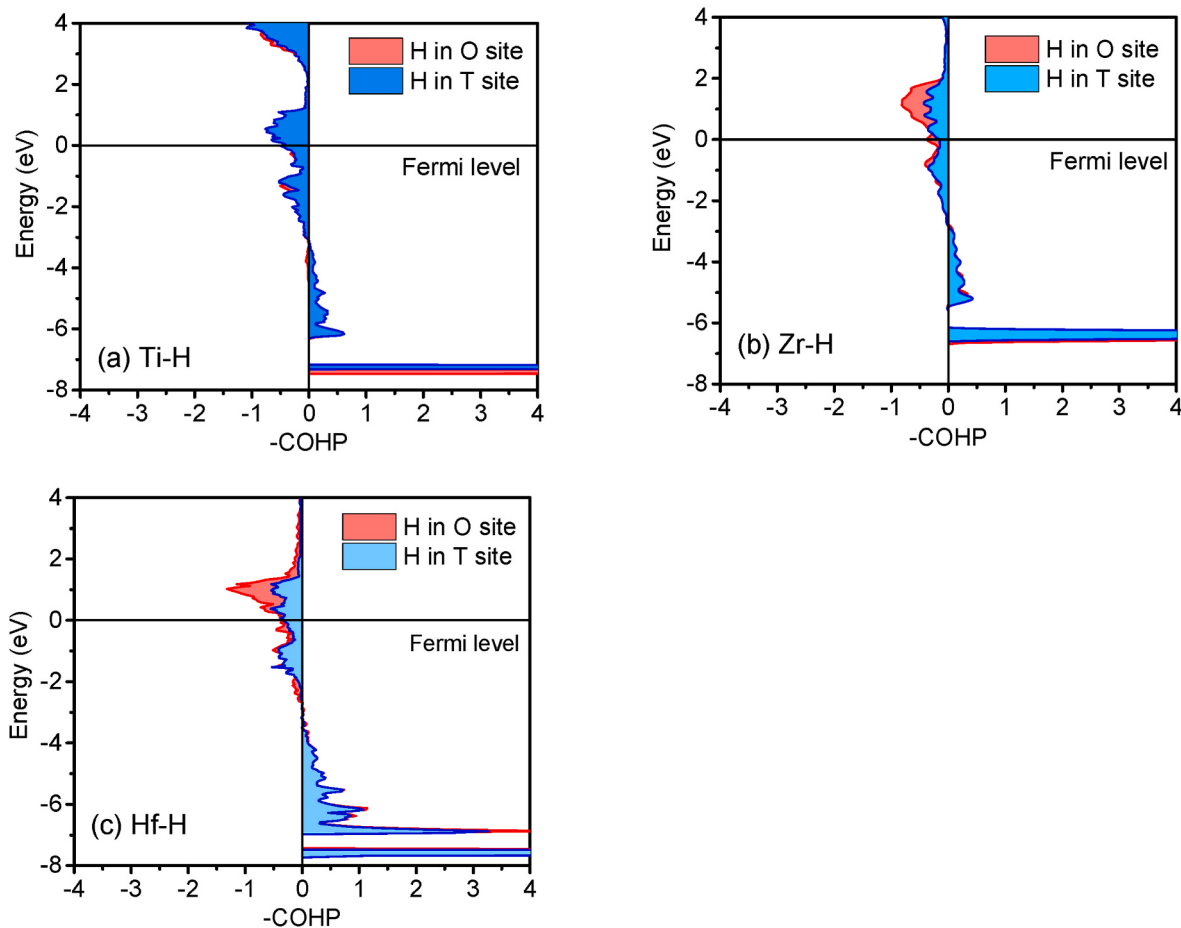


**Fig. 4.** COHP bonding analysis of the shortest M–H bonds with the H atom in the octahedral or tetrahedral interstices for (a) Ti–H (b) Zr–H (c) Hf–H solutions.

increases the electron density over there, i.e., the proton is screened. This is supported by our calculated bonding electron density shown in Fig. 1. Based on such a picture, the heat of formation of a H atom dissolved in a metal may be expressed as

$$E_{\text{sol}} = E_{\text{sol}}^{\text{rep}} + E_{\text{sol}}^{\text{pol}} \quad (6)$$

with the zero-point energy (about 0.05 eV) neglected in the present context [59,60]. Here,  $E_{\text{sol}}^{\text{rep}}$  is the screened proton-ion core interaction of which the major part is the Coulomb repulsion.  $E_{\text{sol}}^{\text{pol}}$  is the energy change on going from the initially electron density without introducing H to the final situation with increasing electron density around the proton.

In general, the proton prefers the interstices with higher electron density (e.g., the T interstice in Ti, Zr, and Hf) to facilitate the accumulation of the electrons around it [62]. However, as seen in Table 2, the size of the T interstice in Ti is smaller than that of the O interstice, which results in stronger Coulomb repulsion between the T-site H (screened proton) and the ions than that between the O-site H and the ions. The stronger Coulomb repulsion makes the T-site less favorable for H. The size of the T interstice in Zr and Hf is also smaller than that of the O interstice, but is larger than that of the T interstice in Ti (at the same level as that of the O interstice in Ti). Therefore, the Coulomb repulsion may not be strong enough to destabilize the T-site H over the O-site H in Zr and Hf.

The validity of the above argument on the distinct site occupations of H in Ti and Zr/Hf may be verified by examining the variation of the site preference of H against the volume (or, say, the size of the interstice) of the system. The stable site (O or T) of H is expected to be reversed with changing volume of the system. For the Ti–H system, an increase in volume leads to a larger T interstice and weaker Coulomb repulsion

between the screened proton and matrix atoms. The Coulomb repulsion for the O-site proton is weakened as well, but the weakening is less strong than that for the T-site proton because the distance between the T-site proton and matrix atom is smaller than that between the O-site proton and matrix atoms while the Coulomb repulsion is in inverse proportional to the square of the distance. Thus, with increasing volume, the T-site should turn to be favorable for H to occupy. On the contrary, for the Zr–H and Hf–H systems, a decrease in volume corresponds to a shrinking T interstice and a stronger Coulomb repulsion, rendering the T-site less favorable for H to occupy.

To confirm the above speculation, the H solution energies against the volume expansion of Ti and contraction of Zr and Hf are calculated as shown in Fig. 5. Here, the volume expansion or contraction is implemented by changing the lattice parameter  $a$  while fixing  $c/a$ . As seen in Fig. 5a, at equilibrium lattice constant ( $a = a_0$  with  $a_0$  being the equilibrium lattice constant), the solution energy of the O-site H is lower than that of the T-site H, i.e., the O-site is preferable for H. With  $a$  expanding by more than about 3%, the solution energy of the T-site H is lower than that of the O-site H, indicating the T-site becomes more stable for H to occupy. For the Zr–H and Hf–H systems, the preferential occupation site for H turns from the T-site at  $a = a_0$  to the O-site for  $a$  shrinking by more than about 1~2%. The above results demonstrate that the Coulomb repulsion between the screened proton and the ions indeed matters for the site occupation of H in Ti, Zr, and Hf.

The energy term  $E_{\text{sol}}^{\text{pol}}$  in Eq. (6), associated with the H-induced electron redistribution, is subtle. The electron redistribution induced by H insertion is expected to have two opposite effects on  $E_{\text{sol}}^{\text{pol}}$ . First, the accumulation of electrons around proton induced by the proton-electron attraction lowers the energy of the M–H system and thus the H solution

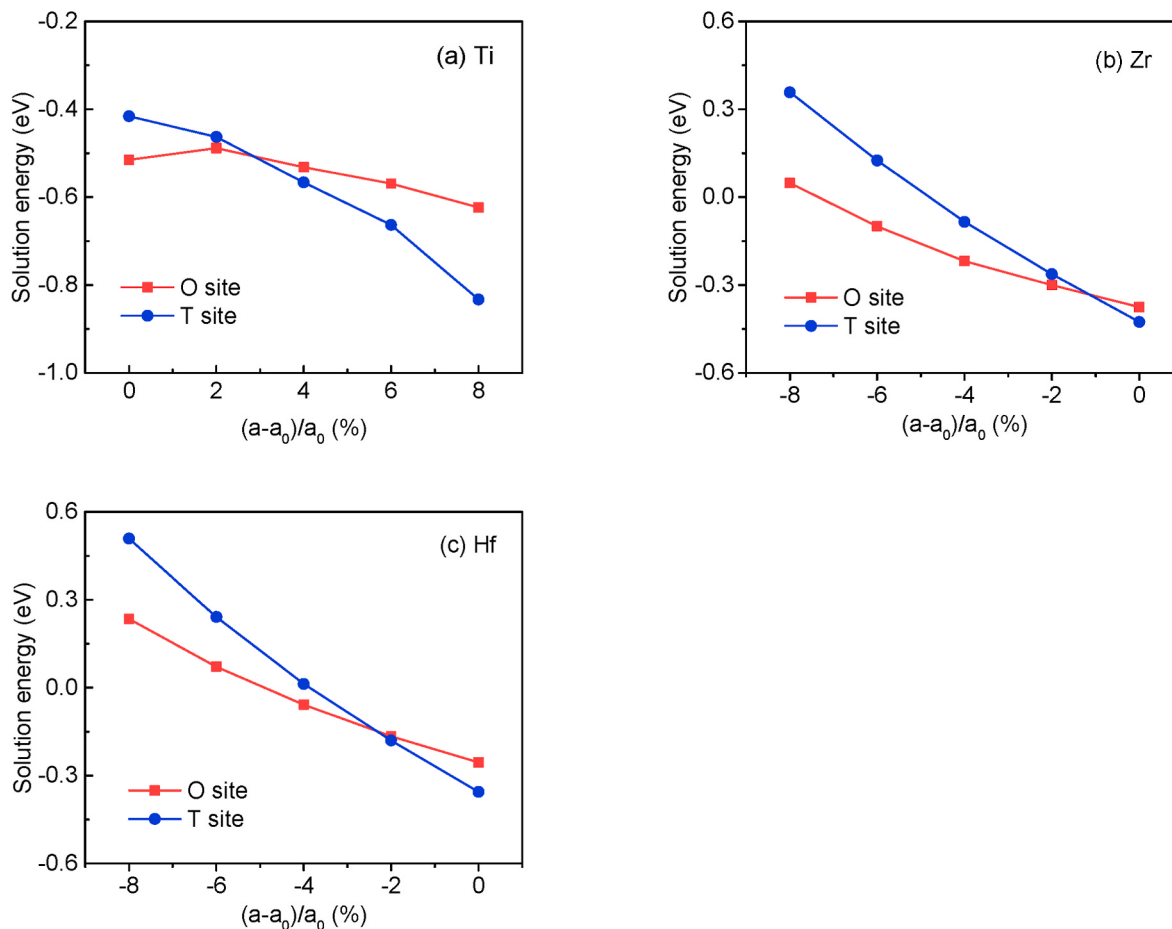


**Fig. 5.** Solution energies of H in the tetrahedral and octahedral interstices of Ti (a), Zr (b), and Hf (c) as functions of the lattice constant expansion/contraction  $(a - a_0)/a$  with  $a$  and  $a_0$  being respectively the expanded/contracted and equilibrium lattice constants. The lattice parameters  $c/a$  for the three systems are fixed at the corresponding equilibrium values.

energy. For all three metals, the bonding electron density in the T interstice is higher than that in the O interstice such that the T-site proton attracts more electrons than the O-site proton (see Fig. 1), indicating that the effect of the accumulation of electrons around the proton favors the T-site H. Second, the electron accumulation leads to the electron depletion outside the screened proton, which weakens the bonding between the matrix atoms such that raises the energy of the system and the H solution energy. For the T-site H, the bonding electrons in the T interstice next to the H atom almost vanishes, i.e., the matrix atoms surrounding the T interstice are debonded. Furthermore, the bonding electron density in the O interstice of the pure Ti/Zr/Hf is much lower than that in the T interstice and the O-site proton attracts less electrons than that in the T-site proton. Consequently, the bonding between the atoms surrounding the O interstice should be less influenced by H dissolving. Therefore, the electron depletion effect should favor the O-site H.

Considering the two opposite effects of the electron redistribution induced by H dissolving, we may argue that, for Ti, the matrix-atom-debonding effect induced by the T-site H is very strong such that the T-site H is destabilized. Due to the high electron density in the O interstice in Ti (relative to that of Zr/Hf), the O-site proton in Ti may still attract enough electrons but with weaker debonding effect than that for the T-site H, which stabilize the O-site H. For Zr and Hf, on the one hand, the matrix-atom-debonding induced by the T-site H is not as strong as that in Ti because the electron density in the T interstice of Zr and Hf is lower than that in Ti. On the other hand, the electron density in the O-site of Zr and Hf is significantly lower than that in Ti such that the O-site proton may not attract enough electrons. Therefore, the T-site H is more

stable than the O-site H. Therefore, the electron redistribution might also contribute to the distinct site occupations of H in Ti and Zr/Hf besides the Coulomb repulsion between the screened proton and metal ions.

The discussed origin of the distinct site occupation of H in Ti and Zr/Hf leads us to an important and general conclusion that H prefers the site with a large space and a high electron density in metals. A larger space corresponds to a weaker proton-ion Coulomb repulsion and matrix-atom debonding effect whereas a higher electron density corresponds to a stronger proton-electron attraction for the clustering of electrons around proton. The two factors are in general contradict to each other. A larger space is generally of a lower electron density. Therefore, the H atom in metal should find the site with a trade-off between a large space and a high electron density.

## 5. Conclusion

First principles calculations demonstrated that the solute H atom occupies octahedral interstice in Ti but tetragonal interstice in Zr and Hf although Ti and Zr/Hf are of the same lattice structure. In the present work, first principles calculations were carefully performed to investigate the distinct site occupations solute H in Ti and Zr/Hf. Our calculations demonstrated that the Ti–H, Zr–H, Hf–H systems share some geometric and electronic structure characteristics.

- smaller size of the T interstice than that of the O interstice;
- larger distortion energy induced by the T-site H than that by the O-site H;

- higher electron density around the T-site H than that around the O-site H;
- higher low-lying DOS for the T-site H than that for the O-site H;
- slightly stronger antibonding character of the M – H bond for the O-site H than that for the T-site H.

However, Ti is different from Zr/Hf in that Ti is more compact than Zr/Hf and the bonding electron density in Ti is significantly higher than that in Zr/Hf. With these two observations and considering that H exists as a screened proton in metals, we propose that the unstable tetrahedral site occupation of H in Ti is ascribed to the strong Coulomb repulsion between the tetrahedral H and its neighboring matrix Ti atoms due to the small interstice size. The debonding of the matrix atoms due to the electron depletion outside the screened proton may also contribute to the less stable tetrahedral H in Ti. The stable tetrahedral site occupation of H in Zr and Hf may be ascribed to the relatively weak Coulomb repulsion because the tetrahedral interstice is relatively large. In the meantime, the proton in tetrahedral interstice of Zr and Hf may attract more electrons than that in the octahedral interstice, which may also make a more stable tetrahedral H than the octahedral H.

Considering the origin of the site preference of H in Ti, Zr, and Hf, we propose that the H atom prefers the site with a large space and a high electron density in metals.

#### CRediT authorship contribution statement

**Fan-Xi Yang:** Writing – original draft, Methodology, Conceptualization. **Yi-Fei Zhu:** Validation, Formal analysis. **Shuo Cao:** Supervision, Conceptualization. **Chao-Ming Wang:** Writing – review & editing, Methodology. **Ying-Jie Ma:** Writing – review & editing, Resources. **Rui Yang:** Writing – review & editing, Resources. **Qing-Miao Hu:** Writing – review & editing, Supervision, Conceptualization.

#### Declaration of competing interest

The authors declare that they have no known competing financial interests or personal relationships that could have appeared to influence the work reported in this paper.

#### Acknowledgement

The authors gratefully acknowledge the financial supports from the National Natural Science Foundation of China (grant Nos. U2106215, 52071315, and 52001307) and the National Key Research and Development Program of China (grant No. 2021YFC2801803).

#### References

- [1] Dwivedi SK, Vishwakarma M. Hydrogen embrittlement in different materials: a review. *Int J Hydrogen Energy* 2018;43(46):21603–16. <https://doi.org/10.1016/j.ijhydene.2018.09.201>.
- [2] Hardie D, Charles EA, Lopez AH. Hydrogen embrittlement of high strength pipeline steels. *Corrosion Sci* 2006;48(12):4378–85. <https://doi.org/10.1016/j.corsci.2006.02.011>.
- [3] Chernov II, Staltssov MS, Kalin BA, et al. Some problems of hydrogen in reactor structural materials: a review. *Inorg Mater. Appl Res* 2017;8(5):643–50. <https://doi.org/10.1134/S2075133117050094>.
- [4] Chang Y, Breen AJ, Tarzimoghadam Z, et al. Characterizing solute hydrogen and hydrides in pure and alloyed titanium at the atomic scale. *Acta Mater* 2018;150: 273–80. <https://doi.org/10.1016/j.actamat.2018.02.064>.
- [5] Lee H, Mall S, Allen WY. Fretting fatigue behavior of shot-peened Ti-6Al-4V under seawater environment. *Mater Sci Eng, A* 2006;420(1–2):72–8. <https://doi.org/10.1016/j.msea.2006.01.031>.
- [6] Wang Z, Garbe U, Li H, et al. Hydrogen-induced microstructure, texture and mechanical property evolutions in a high-pressure torsion processed zirconium alloy. *Scripta Mater* 2012;67(9):752–5. <https://doi.org/10.1016/j.scriptamat.2012.07.033>.
- [7] Ruda M, Bertolino G, Farkas D, et al. Effect of dilute H on crack tip plasticity in Zr. *Comput Mater Sci* 2013;69:327–34. <https://doi.org/10.1016/j.commatsci.2012.11.055>.
- [8] Peters M, Kumpfert J, Ward CH, et al. Titanium alloys for aerospace applications. *Adv Eng Mater* 2003;5(6):419–27. <https://doi.org/10.1002/adem.200310095>.
- [9] Banerjee D, Williams JC. Perspectives on titanium science and technology. *Acta Mater* 2013;61(3):844–79. <https://doi.org/10.1016/j.actamat.2012.10.043>.
- [10] Narang PP, Paul GL, Taylor KNR. Location of hydrogen in  $\alpha$ -zirconium. *J Less-Common Met* 1977;56(1):125–8. [https://doi.org/10.1016/0022-5088\(77\)90225-9](https://doi.org/10.1016/0022-5088(77)90225-9).
- [11] Fukai Y. The metal-hydrogen system: basic bulk properties. New York: Springer; 2009.
- [12] Domain C, Besson R, Legris A. Atomic-scale Ab-initio study of the Zr-H system I. Bulk properties. *Acta Mater* 2002;50(14):3513–26. [https://doi.org/10.1016/S1359-6454\(02\)00173-8](https://doi.org/10.1016/S1359-6454(02)00173-8).
- [13] Holliger L, Legris A, Besson R. Hexagonal-based ordered phases in H-Zr. *Phys Rev B* 2009;80(9):094111. <https://doi.org/10.1103/PhysRevB.80.094111>.
- [14] Varvenne C, Mackin O, Provile L, et al. Hydrogen and vacancy clustering in zirconium. *Acta Mater* 2016;102:56–69. <https://doi.org/10.1016/j.actamat.2015.09.019>.
- [15] Wang J, Shao B, Shan D, et al. Effect of strain on solution energy of hydrogen in alpha-zirconium from first-principle calculations. *Int J Hydrogen Energy* 2020;45(35):18001–9. <https://doi.org/10.1016/j.ijhydene.2020.04.244>.
- [16] Song Y, Yang R, Li D, et al. A first-principles study of the theoretical strength and bulk modulus of hcp metals. *Philos Mag A* 2001;81(2):321–30. <https://doi.org/10.1080/01418610108214306>.
- [17] Mintz MH. Hafnium-hydrogen. *Solid State Phenom* 1996;49–50:331–56. <https://doi.org/10.4028/www.scientific.net/SSP.49-50.331>.
- [18] Xiao W, Sun L, Huang S-H, et al. Stability and mechanical properties of various Hf-H phases: a density-functional theory study. *Chin Phys B* 2017;26(10):106103. <https://api.semanticscholar.org/CorpusID:250912831>.
- [19] Khoda-Bakhsh R, Ross DK. Determination of the hydrogen site occupation in the  $\alpha$  phase of zirconium hydride and in the  $\alpha$  and  $\beta$  phases of titanium hydride by inelastic neutron scattering. *J Phys F Met Phys* 1982;12:15–24. <https://doi.org/10.1088/0305-4608/12/1/003>.
- [20] Pinto H, Korn C, Goren S, et al. Neutron diffraction study of hydrogen in  $\alpha$  titanium. *Solid State Commun* 1979;32(5):397–8. [https://doi.org/10.1016/0038-1098\(79\)90474-5](https://doi.org/10.1016/0038-1098(79)90474-5).
- [21] Korn C, Zamir D, Hadari Z, et al. Hydrogen in Ti-V alloys. *Phys Status Solidi B* 1975;32(2):K147–50. <https://doi.org/10.1002/pssa.2210320260>.
- [22] Hempelmann R, Richter D, Stritzker B. Optic phonon modes and superconductivity in  $\alpha$  phase (Ti, Zr)-(H, D) alloys. *J Phys F Met Phys* 1982;12:79–86. <https://doi.org/10.1088/0305-4608/12/1/009>.
- [23] Alperin HA, Flotow H, Rush JJ, et al. Deuterium-site occupancy in the  $\alpha$  and  $\beta$  phases of TiD<sub>x</sub>. *Proceedings of the conference on neutron scattering*. Gatlinburg, Tennessee; 1976.
- [24] Matsumoto R, Sera M, Miyazaki N. Hydrogen concentration estimation in metals at finite temperature using first-principles calculations and vibrational analysis. *Comput Mater Sci* 2014;91:211–22. <https://doi.org/10.1016/j.commatsci.2014.04.051>.
- [25] Poletaev DO, Aksyonov DA, Vo DD, et al. Hydrogen solubility in hcp titanium with the account of vacancy complexes and hydrides: a DFT study. *Comput Mater Sci* 2016;114:199–208. <https://doi.org/10.1016/j.commatsci.2015.12.037>.
- [26] Wang C-M, Cao S, Yang F-X, et al. Insights into the formation of titanium hydrides from first principles calculations. *Acta Mater* 2024;272:119921. <https://doi.org/10.1016/j.actamat.2024.119921>.
- [27] Xiao HZ. On the mechanism of hydride formation in  $\alpha$ -Ti alloys. *Scripta Metall Mater* 1992;27(5):571–6. [https://doi.org/10.1016/0956-716X\(92\)90342-C](https://doi.org/10.1016/0956-716X(92)90342-C).
- [28] Howe JM, Tsai MM. Discussion of “on the mechanism of hydride formation in  $\alpha$ -Ti alloys” Xiao HZ, editor. *Scripta Metall Mater* 1993;28(4):533–5. [https://doi.org/10.1016/0956-716X\(93\)90096-B](https://doi.org/10.1016/0956-716X(93)90096-B).
- [29] Numakura H, Koiba M. Hydride precipitation in titanium. *Acta Metall* 1984;32(10):1799–807. [https://doi.org/10.1016/0001-6160\(84\)90236-0](https://doi.org/10.1016/0001-6160(84)90236-0).
- [30] Novoselov II, Yanilkin AV. Hydrogen diffusion in titanium dihydrides from first principles. *Acta Mater* 2018;153:250–6. <https://doi.org/10.1016/j.actamat.2018.04.059>.
- [31] Li J, Li X, Sui M. Formation mechanism of hydride precipitation in commercially pure titanium. *J Mater Sci Technol* 2021;81:108–16. <https://doi.org/10.1016/j.jmst.2021.01.009>.
- [32] Majer G, Renz W, Barnes RG. The mechanism of hydrogen diffusion in zirconium dihydrides. *J Phys Condens Matter* 1994;6:2935–42. <https://doi.org/10.1088/0953-8984/6/15/015>.
- [33] Liang CP, Gong HR. Fundamental mechanism of tetragonal transitions in titanium hydride. *Mater Lett* 2014;115:252–5. <https://doi.org/10.1016/j.mallet.2013.10.091>.
- [34] Liang CP, Gong HR. Atomic structure, mechanical quality, and thermodynamic property of TiH<sub>x</sub> phases. *J Appl Phys* 2013;114(4):043510. <https://doi.org/10.1063/1.4816485>.
- [35] El-Ghobashy M, Hashim H, Darwish M, et al. Eco-friendly NiO/polydopamine nanocomposite for efficient removal of dyes from wastewater. *Nanomaterials* 2022;12(7). <https://doi.org/10.3390/nano12071103>.
- [36] Henaiash AM, Darwish MA, Hemeda OM, et al. Structure and optoelectronic properties of ferroelectric PVA-PZT nanocomposites. *Opt Mater* 2023;138. <https://doi.org/10.1016/j.optmat.2022.113402>.
- [37] Hussein MM, Saafan SA, Abosheisha HF, et al. Structural and dielectric characterization of synthesized nano-BSTO/PVDF composites for smart sensor applications. *Mater Adv* 2023;4(22):5605–17. <https://doi.org/10.1039/D3MA00437F>.

- [38] Hussein MM, Saafan SA, Abosheisha HF, et al. Preparation, structural, magnetic, and AC electrical properties of synthesized CoFe2O4 nanoparticles and its PVDF composites. *Mater Chem Phys* 2024;317. <https://doi.org/10.1016/j.matchemphys.2024.129041>.
- [39] Migas DB, Turchenko VA, Rutkauskas AV, et al. Temperature induced structural and polarization features in BaFe12O19. *J Mater Chem C* 2023;11(36):12406–14. <https://doi.org/10.1039/D3TC01533E>.
- [40] Tishkevich DI, Grabchikov SS, Lastovskii SB, et al. Function composites materials for shielding applications: correlation between phase separation and attenuation properties. *J Alloys Compd* 2019;771:238–45. <https://doi.org/10.1016/j.jallcom.2018.08.209>.
- [41] Trukhanov SV, Fedotova VV, Trukhanov AV, et al. Cation ordering and magnetic properties of neodymium-barium manganites. *Tech Phys* 2008;53(1):49–54. <https://doi.org/10.1134/S106378420801009X>.
- [42] Trukhanov AV, Tishkevich DI, Timofeev AV, et al. Structural and electrodynamic characteristics of the spinel-based composite system. *Ceram Int* 2024;50(12):12131–7. <https://doi.org/10.1016/j.ceramint.2024.03.241>.
- [43] Trukhanov AV, Turchenko VO, Bobrikov IA, et al. Crystal structure and magnetic properties of the BaFe<sub>12-x</sub>Al<sub>x</sub>O<sub>19</sub> (x=0.1–1.2) solid solutions. *J Magn Magn Mater* 2015;393:253–9. <https://doi.org/10.1016/j.jmmm.2015.05.076>.
- [44] Trukhanov SV, Trukhanov AV, Vasiliev AN, et al. Frustrated exchange interactions formation at low temperatures and high hydrostatic pressures in La<sub>0.7</sub>Sr<sub>0.3</sub>MnO<sub>2</sub>.85. *J Exp Theor Phys* 2010;111(2):209–14. <https://doi.org/10.1134/S106377611008008X>.
- [45] Trukhanov SV, Zubar TI, Turchenko VA, et al. Exploration of crystal structure, magnetic and dielectric properties of titanium-barium hexaferrites. *Mater Sci Eng, B* 2021;272. <https://doi.org/10.1016/j.mseb.2021.115345>.
- [46] Vinnik DA, Starikov AY, Zhivulin VE, et al. Changes in the structure, magnetization, and resistivity of BaFe<sub>12-x</sub>Ti<sub>x</sub>O<sub>19</sub>. *ACS Appl Electron Mater* 2021;3(4):1583–93. <https://doi.org/10.1021/acsaelm.0c01081>.
- [47] Zhivulin VE, Trofimov EA, Zaitseva OV, et al. Preparation, phase stability, and magnetization behavior of high entropy hexaferrites. *iScience* 2023;26(7). <https://doi.org/10.1016/j.isci.2023.107077>.
- [48] Kresse G, Furthmüller J. Efficiency of ab-initio total energy calculations for metals and semiconductors using a plane-wave basis set. *Comput Mater Sci* 1996;6(1):15–50. [https://doi.org/10.1016/0927-0256\(96\)00008-0](https://doi.org/10.1016/0927-0256(96)00008-0).
- [49] Kresse G, Joubert D. From ultrasoft pseudopotentials to the projector augmented-wave method. *Phys Lett B* 1999;59(3):1758–75. <https://doi.org/10.1016/PhysRevB.59.1758>.
- [50] Perdew JP, Burke K, Ernzerhof M. Generalized gradient approximation made simple. *Phys Rev Lett* 1996;77(18):3865–8. <https://doi.org/10.1103/PhysRevLett.77.3865>.
- [51] Perdew JP, Ruzsinszky A, Csonka GI, et al. Restoring the density-gradient expansion for exchange in solids and surfaces. *Phys Rev Lett* 2008;100(13):136406. <https://doi.org/10.1103/PhysRevLett.100.136406>.
- [52] Perdew JP, Chevary JA, Vosko SH, et al. Atoms, molecules, solids, and surfaces: applications of the generalized gradient approximation for exchange and correlation. *Phys Rev B* 1992;46(11):6671–87. <https://doi.org/10.1103/PhysRevB.46.6671>.
- [53] Hammer B, Hansen LB, Nørskov JK. Improved adsorption energetics within density-functional theory using revised Perdew-Burke-Ernzerhof functionals. *Phys Rev B* 1999;59(11):7413–21. <https://doi.org/10.1103/PhysRevB.59.7413>.
- [54] Maintz S, Deringer VL, Tchougréeff AL, et al. Analytic projection from plane-wave and PAW wavefunctions and application to chemical-bonding analysis in solids. *J Comput Chem* 2013;34(29):2557–67. <https://doi.org/10.1002/jcc.23424>.
- [55] Maintz S, Deringer VL, Tchougréeff AL, et al. LOBSTER: a tool to extract chemical bonding from plane-wave based DFT. *J Comput Chem* 2016;37(11):1030–5. <https://doi.org/10.1002/jcc.24300>.
- [56] Liang CP, Gong HR. Fundamental influence of hydrogen on various properties of  $\alpha$ -titanium. *Int J Hydrogen Energy* 2010;35(8):3812–6. <https://doi.org/10.1016/j.ijhydene.2010.01.080>.
- [57] Yamanaka S, Higuchi K, Miyake M. Hydrogen solubility in zirconium alloys. *J Alloys Compd* 1995;231(1–2):503–7. [https://doi.org/10.1016/0925-8388\(95\)01864-6](https://doi.org/10.1016/0925-8388(95)01864-6).
- [58] Fisher ES, Renken CJ. Single-crystal elastic moduli and the hcp  $\rightarrow$  bcc transformation in Ti, Zr, and Hf. *Phys Rev* 1964;135(2A):A482–94. <https://doi.org/10.1103/PhysRev.135.A482>.
- [59] Ebisuzaki Y, O'Keeffe M. The solubility of hydrogen in transition metals and alloys. *Prog Solid State Chem* 1967;4:187–211. [https://doi.org/10.1016/0079-6786\(67\)90008-8](https://doi.org/10.1016/0079-6786(67)90008-8).
- [60] Oates WA, Flanagan TB. The solubility of hydrogen in transition metals and their alloys. *Prog Solid State Chem* 1981;13(3):193–283. [https://doi.org/10.1016/0079-6786\(81\)90002-9](https://doi.org/10.1016/0079-6786(81)90002-9).
- [61] Zamir D. Nuclear-magnetic-resonance study of hydrogen alloying in the early transition metals (group VB). *Phys Rev* 1965;140(1A):A271–4. <https://doi.org/10.1103/PhysRev.140.A271>.
- [62] Xing W, Chen X-Q, Li X, et al. First-principles study of hydrogen trapping behavior in face centered cubic metals (M=Ni, Cu and Al) with monovacancy. *Int J Hydrogen Energy* 2020;45(46):25555–66. <https://doi.org/10.1016/j.ijhydene.2020.06.266>.